Dissipative Dynamics of Graph-State Stabilizers with Superconducting Qubits

Liran Shirizly[1,*] Grégoire Misguich,[2,†] and Haggai Landa[1,‡]

[1]*IBM Quantum, IBM Research - Israel, Haifa University Campus, Mount Carmel, Haifa 31905, Israel*
[2]*Université Paris-Saclay, CNRS, CEA, Institut de Physique Théorique, 91191 Gif-sur-Yvette, France*

We study experimentally and numerically the noisy evolution of multipartite entangled states, focusing on superconducting qubit devices accessible via the cloud. We find that a valid modeling of the dynamics requires one to properly account for coherent frequency shifts, caused by stochastic charge-parity fluctuations. We introduce an approach modeling the charge-parity splitting using an extended Markovian environment. This approach is numerically scalable to tens of qubits, allowing us to simulate efficiently the dissipative dynamics of some large multiqubit states. Probing the continuous-time dynamics of increasingly larger and more complex initial states with up to 12 coupled qubits in a ring-graph state, we obtain a good agreement of the experiments and simulations. We show that the underlying many-body dynamics generate decays and revivals of stabilizers, which are used extensively in the context of quantum error correction. Furthermore, we demonstrate the mitigation of 2-qubit coherent interactions (crosstalk) using tailored dynamical decoupling sequences. Our noise model and the numerical approach can be valuable to advance the understanding of error correction and mitigation and invite further investigations of their dynamics.

State-of-the-art qubit devices for quantum computation have been realized with tens and hundreds of qubits on single chips [1–4]. In many of those devices the models describing the control and environment errors are often similar, even when the underlying physical mechanisms are quite different. The noise sensitivity of the individual qubits and gate operations make quantum error correction codes an essential goal in the field, en route to harnessing the full power of quantum algorithms [5–11].

Many quantum codes are based on storing information in delocalized, entangled N-qubit states ($N \gg 1$), and measuring n-qubit (nQ) operators (of low weight, $n \ll N$) for the detection of local errors and the application of corrections. A lot of effort is devoted to the development of numerical tools and characterization procedures, focusing both on the microscopic qubit dynamics and the high-level gates, and the question of whether the noise is Markovian (memoryless) or the contrary [12–23]. In general, it is hard to model faithfully the interplay of various decoherence mechanisms and the continuous dynamics of coupled qubits. One of the outstanding challenges is the incorporation of noise parameters measured at the few-qubits level, in the regime of multiqubit-state dynamics.

In this Letter, we develop a fundamental noise model that is extensible to the many-body regime of qubit dynamics. We experimentally and numerically study the continuous-time dynamics of multiqubit graph states [24,25]. Our experiments are conducted using *qiskit-experiments* [26] on IBM Quantum superconducting transmon qubits accessible via the cloud [27]. We characterize the $1Q$ and $2Q$ parameters relevant in the studied setup, together with state

preparation and measurement (SPAM) errors. Identifying errors that may appear non-Markovian, but can in fact be described using an appropriate Markovian environment, we employ a high-performance numerical solver [28–30] that allows us to efficiently handle the density matrix of many-qubit states. The simulation gives us access to state characteristics that are otherwise inaccessible.

Figure 1 shows a schematic depiction of the setup studied in this Letter. The dynamical model that we
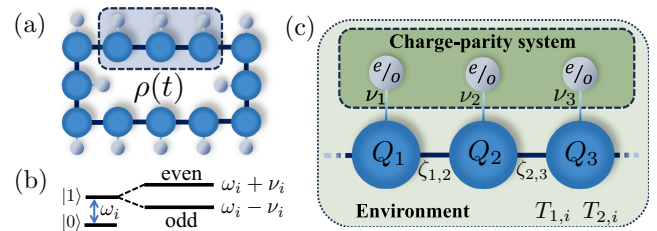

FIG. 1. (a) This Letter focuses on the dynamics of an open quantum system with a density matrix $\rho(t)$ of 12 qubits in a ring. (b) For superconducting qubits, the qubit levels (with frequency ω_i) are split due to charge-parity fluctuations that manifest effectively as a Bernoulli stochastic variable shifting the qubit frequency by $\pm\nu_i$. (c) To model the charge-parity splitting in a many-body simulation reproducing the experiment dynamics, each qubit Q_i is coupled to a fictitious two-level system [with levels denoted by e, o (even, odd)] initialized to a diagonal mixed state, which is traced over at the end of a calculation. The model further includes energy relaxation time ($T_{1,i}$), dephasing time ($T_{2,i}$), and 2-qubit ZZ crosstalk ($\zeta_{i,j}$)—see the text for details.

consider applies generally to the decoherence of quantum memory states relevant for many physical systems. We start from the term in the dynamics specific to superconducting qubits, describing charge-parity oscillations. In essence, each qubit's frequency is shifted according to the charge parity (even or odd) of the qubit's junction electrodes, which switches due to quasiparticle tunneling. This splitting has been treated in the context of single-qubit experiments [31–38], and in this Letter we present an approach for its inclusion as part of the basic noise model of many-body dynamics of superconducting qubits, essential for accurate simulations.

As an example demonstrating the parity oscillations of a single qubit we consider a simple Ramsey experiment, wherein a qubit is prepared in the $|+\rangle = (|0\rangle + |1\rangle)/\sqrt{2}$ state (along the $+x$ direction of the Bloch sphere), and then its time evolution is probed with measurements in the x, y, and z bases repeatedly to collect the probability of measuring the positive eigenstate. The magnitude of the qubit's Bloch vector projection on the xy plane is plotted in Fig. 2(a) as a function of the time, together with $\langle z \rangle$. Here and in the rest of the Letter, experimental data points and error bars indicate the mean and 1 standard deviation of 1024 measurements (shots) [39]. The observed oscillations of the qubit's Bloch vector norm could be assumed to result from an interaction (with a neighboring qubit or an uncontrolled degree of freedom) or a non-Markovian noise process, but this is, in fact, not the case here.
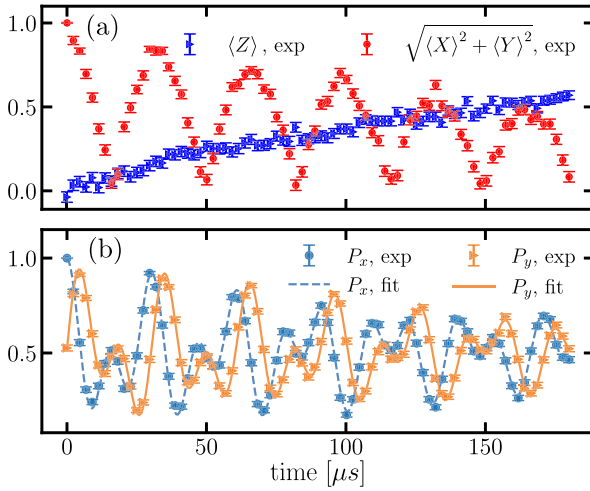

FIG. 2. (a) A single qubit's mean xy projection of the Bloch vector ($\sqrt{\langle X \rangle^2 + \langle Y \rangle^2}$) as a function of time after being initialized to the $|+\rangle$ state in a Ramsey experiment, plotted together with $\langle Z \rangle$ whose amplitude grows as the qubit's ground state becomes populated at a rate equal to $1/T_1$. The shrinking of the xy projection and its revival is reminiscent of a non-Markovian process. (b) A characterization of ν and Δ of Eq. (1) together with the decoherence time T_2 from the data points in an identical Ramsey experiment with the lines showing a fit of the data according to Eqs. (2) and (3).

With superconducting qubit devices, each qubit's frequency is first characterized to determine the microwave drive frequency to which each qubit is locked in experiments to follow. In the rotating frame with respect to this predetermined frequency, each of the parity states (denoted hereafter by a subscript $a \in \{e, o\}$) is subject to a Hamiltonian with a shifted frequency,

$$H_a/\hbar = \frac{1}{2}\omega_a(1 - \sigma^z), \quad \omega_e = \Delta + \nu, \quad \omega_o = \Delta - \nu, \quad (1)$$

where Δ is the mean drift (or detuning) of the qubit's frequency from the microwave frame fixed previously, and ν the parity oscillations' frequency. Equation (1) adopts the convention that the qubit's ground state obeys $\sigma^z|0\rangle = |0\rangle$, while for the excited state $\sigma^z|1\rangle = -|1\rangle$, and the higher levels beyond the first two are neglected.

The probabilities of even and odd parities have been taken in earlier experiments as being equal over appropriate time-scales [34–37]. We test the consistency of this assumption with our model in the current device. Assuming that during each shot of the experiment the qubit's charge parity is even or odd but constant, its density matrix $\rho(t)$ can be described as a convex sum of the independent parity contributions, $\rho = b\rho_e + (1 - b)\rho_o$, where we introduce b to parametrize the fraction of shots with even parity. By fitting b as a free parameter, we find that $b \approx 0.5$ almost always (within statistical noise), although we also find rare deviations (see Supplemental Material [41]). We set $b = 1/2$ hereafter, describing well our data.

Figure 2(b) presents an example of a similar Ramsey experiment as described above, fitting the parameters of Eq. (1) using the probabilities of measurements along the x and y directions. Each of the signals can be written as the product of two decaying oscillations [41],

$$P_x = A \exp(-t/T_2) \cos[(\Delta + \omega_s)t + \phi] \cos(\nu t) + B, \quad (2)$$

$$P_y = A \exp(-t/T_2) \sin[(\Delta + \omega_s)t + \phi] \cos(\nu t) + B, \quad (3)$$

where ω_s is the "intended" frame detuning offset added to improve the signal, and T_2 is the dephasing time. In addition ϕ, A, and B are fitting parameters accounting for the SPAM errors, which ideally would be 0, 1/2, and 1/2, respectively. We find that the model is consistent with the experiment data without requiring an additional Gaussian decay envelope corresponding to a $1/f$ noise [41,42]. The characterized values of ν are consistent with the theoretical charge dispersion [43,44] of our used transmon qubits [41].

Once ν is characterized for each qubit, the Hamiltonians H_e and H_o can be constructed numerically and the dynamics of the system can be simulated. However, an N-qubit simulation accounting for the charge-parity splitting would have to average the results of 2^N different time

evolutions with their modified parameters corresponding to the initial conditions of even or odd parity. This quickly becomes intractable, and here we choose instead a different approach that allows us to scale our simulations to tens of qubits under relevant conditions. For the purpose of simulation, we can map the problem of a qubit whose frequency is a (Bernoulli) random variable onto an open system with an additional fictitious "qubit" whose ground state labels the even parity, while its excited state relates to the odd parity. The Hamiltonian of the system can then be written as

$$H_1/\hbar = \frac{1}{2}\sum_i [\Delta_i + \nu_i \tilde{\sigma}_i^z](1 - \sigma_i^z), \qquad (4)$$

where σ_i^z is the Pauli z matrix of the actual qubit, and $\tilde{\sigma}_i^z$ is the Pauli z matrix corresponding to the parity. The parity qubit can be described by a diagonal density matrix (parametrized with b), which naturally remains invariant under the time evolution. In this approach, the system dimension apparently increases (exponentially) as compared with sampling of simulations with even and odd parameters. However, the Hamiltonian in Eq. (4) is naturally suitable for a solver based on matrix product states (MPSs) and matrix product operators, since the fictitious qubits do not develop entanglement with the system qubits and only increase the computational requirements by a small amount.

In addition to the one-body Hamiltonian of Eq. (4), we run standard characterization experiments of the effective (approximate) ZZ interaction strength of every pair of idle qubits connected according to the device topology, taking the form [45,46]

$$H_2/\hbar = \frac{1}{2}\sum_{\langle i,j \rangle} \zeta_{ij}(1 - \sigma_i^z)(1 - \sigma_j^z), \qquad (5)$$

where the summation is over the nearest neighbors. The total Hamiltonian of the idle qubits is therefore $H = H_1 + H_2$. To gain some understanding of the Hamiltonian dynamics, we consider the effect of tracing out all qubits except qubit i, which has n_i nearest neighbors. The resulting $1Q$ density matrix evolution can be described as a mixture of 2^{1+n_i} effective qubits (see Supplemental Material [41]), each oscillating coherently with different frequency $\omega_i \in \{\Delta_i \pm \nu_i + \sum_j (1 \pm 1)\zeta_{ij}\}$, where the sum is over the qubit's neighbors.

Incorporating the dissipative dynamics is more complex [47] and, to capture the full dynamics, evolved numerical tools are needed [29,48]. We solve a Lindblad master equation for $\rho(t)$, accounting for evolution with the Hamiltonian H together with standard noise operators fed with the T_1 (lifetime due to spontaneous emission toward the ground state) and T_2 values of each qubit,

$$\partial_t \rho = -\frac{i}{\hbar}[H, \rho] + \mathcal{D}[\sigma^+] + \mathcal{D}[\sigma^z]. \qquad (6)$$

In Eq. (6) the dissipators take a standard form, $\mathcal{D}[\sigma^+]$ describes relaxation (spontaneous emission) toward each qubit's ground state, and $\mathcal{D}[\sigma^z]$ describes dephasing [41]. We have validated that a heating term can be neglected, since under typical conditions of superconducting qubits it is significantly suppressed [41]. The initial state in the experiment is characterized accurately (self-consistently) and fed into the simulation, parametrized for each qubit by the three Bloch vector coordinates [49]. Single-qubit readout errors are accounted for and mitigated (in the mean) in the experimental results by assuming uncorrelated errors, observed to be a very good approximation in current devices [49,50]. The continuous dynamics together with intermediate gates are solved with a high precision (see Supplemental Material [41]).

In the rest of this Letter, we describe the results of experiments and simulations probing the dynamics of increasingly larger and more complex initial states. The parameters $\{\nu_i, \Delta_i, T_{1,i}, T_{2,i}, \zeta_{i,j}\}$ and SPAM parameters are determined by characterization experiments. We use the mean values of the estimated parameters for the simulations. The values are given in [41]. In Fig. 3(a) we plot the time evolution of the middle qubit of three, initialized and simulated starting from the product state $|+\rangle^{\otimes 3}$. The choice
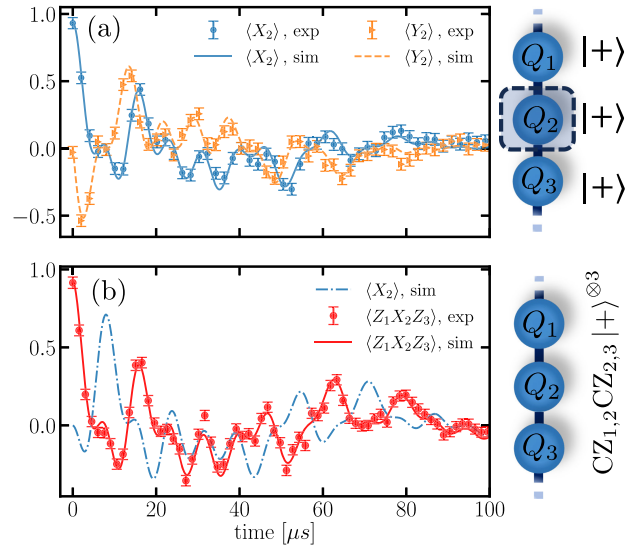

FIG. 3. (a) Dynamics of the middle qubit among three that are initialized to the product state $|+\rangle^{\otimes 3}$. The experiment measurements are given by the points (with statistical error bars) and the lines are taken from simulation data. The multiple frequencies visible in the oscillations of the shown qubit result from the combination of its parity oscillations, detuning error, and ZZ coupling to two neighbors (with different coupling strengths)— see the text for a detailed discussion. (b) The dynamics of the $Z_1 X_2 Z_3$ stabilizer of a similar $3Q$ chain initialized in a graph state and of the middle qubit's $\langle X \rangle$. In this figure and in Fig. 4, the lines show simulation data that, once the Hamiltonian and noise parameters have been determined, do not involve any adjustable parameters.

of an initial state in the equatorial plane of the Bloch sphere reveals the presence of multiple frequencies in the dynamics, visible in Fig. 3(a). Because of the ZZ coupling, the qubits develop some entanglement, while the competing incoherent processes damp the oscillations. The simulation captures this dynamics very precisely, and this is the result of focusing on data with a successful fitting of the parameters and the absence of drifts and jumps over the experiment duration or interactions with uncontrolled degrees of freedom (see Ref. [41]).

In the next step, we perform a similar experiment and simulation, replacing the initial state by a 3-qubit linear graph state, which is equivalent up to local rotations to a Greenberger-Horne-Zeilinger (GHZ) state [51], a maximally entangled state of three qubits. This graph state can be written explicitly as $|g\rangle = (CZ_{1,2}CZ_{2,3})|+\rangle^{\otimes 3}$, where $CZ_{i,j}$ is the controlled-Z gate applied to qubits i and j. An N-qubit graph state can be characterized also as the unique eigenstate of all N stabilizers with an eigenvalue 1, i.e., $S_k|g\rangle = |g\rangle$, where S_k is a stabilizer of the graph state if it is the product of an X operator on qubit k and Z operators on all of its neighbors in the graph [24]. As in quantum error correction, these stabilizers generate a commutative subgroup of the Pauli group that does not contain $-\mathbb{1}$ [52]. In Fig. 3(b) we present the dynamics of the stabilizer $S_2 = Z_1X_2Z_3$ of the initial graph, where in this notation a capitalized letter from $\{X, Y, Z, I\}$ identifies a Pauli matrix or the identity, and the index indicates the qubit. The initial value of the stabilizer $\langle Z_1X_2Z_3\rangle$ in Fig. 3(b) differs from 1 in our experiments due to preparation errors (see Supplemental Material [41]). At intermediate times, the stabilizer's oscillations are closely related to those of $\langle X_2\rangle$, which result from the combination of all Hamiltonian parameters as discussed above.

We now turn to the largest setup studied in this Letter and our main result. We consider the dynamics of 12 qubits in a ring topology found in current IBM Quantum devices [27,53–56], as depicted schematically in Fig. 1(a). On such a ring, a translation-invariant graph state can be created efficiently using two layers of parallel CZ gates [41], minimizing the initialization errors. The 12 state stabilizers are $Z_{i-1}X_iZ_{i+1}$, where the X_i operator is shifted along all qubits, and their expectation value can be measured using just two measurement setups, $X_1Z_2X_3Z_4...X_{11}Z_{12}$ and $Z_1X_2Z_3X_4...Z_{11}X_{12}$, and then tracing out the irrelevant qubits [57]. This makes the (destructive) characterization of the state using its stabilizers very practical experimentally, and the relevance of the local stabilizers for characterizing complex states is well motivated in the context of error correction codes. In Fig. 4(a) we present a global measure of the deviation of the 12 stabilizers from their ideal expectation value of 1, derived by averaging over the positive quantities $(1 + \langle S_i\rangle)/2$, giving the mean of the corresponding projection operators, to define $\bar{P} = (1/N)\times \sum_i \frac{1}{2}(1 + \langle S_i\rangle)$. In the equilibrium (steady) state to which
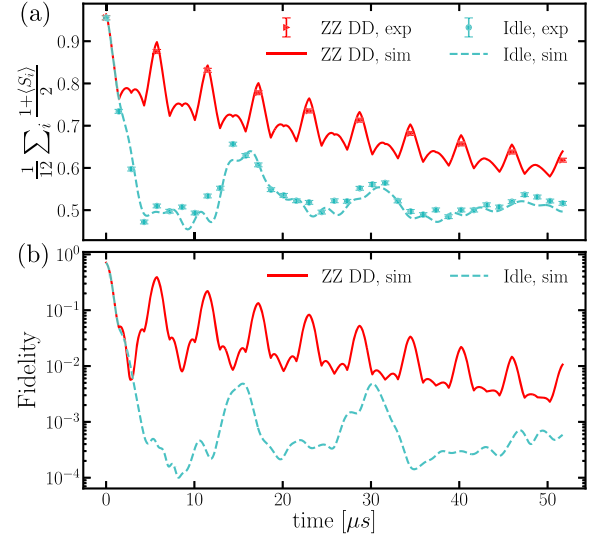

FIG. 4. (a) The dynamics of the $12Q$-ring graph-state stabilizers' mean decoherence, as measured in the experiment (points) and extracted from simulations (lines). The presented measure that ideally equals 1 is shown with and without intermediate dynamical decoupling sequences, which cancel the effect of frequency shifts, charge-parity fluctuations, and ZZ coupling; see the text for details. (b) Using the data of the same simulations, we can see how the fidelity of $\rho(t)$ with the ideal $12Q$ state is significantly improved when using the DD sequence canceling the coherent Hamiltonian errors.

the system approaches for $t \gg T_{1,i}$ (which is close to the Hamiltonian ground state), we have $\langle Z_{i-1}X_iZ_{i+1}\rangle = 0$ for all stabilizers. Therefore, $\bar{P} = 1$ is the ideal case of a perfect pure state, while in the ground state $\bar{P} = 1/2$. The presented experimental dynamics of $\bar{P}$ are reproduced well in the simulation, and the individual 12 stabilizers are shown in the Supplemental Material [41].

A natural next step is to consider the effect of dynamical decoupling (DD) in the current experiment. As follows from Eq. (1), both the detuning (frame) errors and parity oscillations can be canceled by standard $1Q$ DD sequences. The ZZ (crosstalk) interactions can be treated in parallel by staggering the single-qubit X gates across the device according to a two coloring of the interaction edges (a similar protocol including Y gates has been demonstrated in [58]). The total delay time T_{final} is sliced to $n_{\text{DD}} = T_{\text{final}}/T$ repetitions of DD sequences. Within each slice of delay time T, an X gate is applied on each of the qubits of the first colored subgraph at times $T/2$ and T, and on the second subgraph the X gates are applied at $T/4$ and $3T/4$ [41]. Figure 4(a) shows the stabilizer dynamics obtained by adding this DD sequence. We measure the state at several different times $n_{\text{DD}}T$ according to the number of DD repetitions $n_{\text{DD}} = 0, 1, ..., 9$ with constant time slices T. Compared with the idle data, we measure less points in order to reduce the amount of error introduced into the experiment by the DD gates themselves (which can result,

e.g., from gate inaccuracies, leakage of qubit wave functions out of the qubit manifold, and induced interactions). The improvement in $\bar{P}$ is clear and consistent. Although not all measured stabilizers agree exactly with the simulated ones (as can be seen by examining each of them in the Supplemental Material [41], where we discuss in more detail the discrepancies), the high degree of correspondence makes it plausible that the simulations capture the hardware dynamics to a large extent. This gives us a new powerful tool allowing us to calculate nonlocal quantities that are hard to track experimentally. As an example, we take the data from the same simulations described above and show in Fig. 4(b) the evolution of the full many-body fidelity of the noisy state with the ideal intended graph state. The fidelity is very sensitive to errors and the simulations indicate an improvement by about 2 orders of magnitude with the DD sequence.

To conclude, we have demonstrated the characterization of noisy dynamics of multipartite entangled states of superconducting qubits, together with a model and a numerical approach allowing for an accurate corresponding simulation. We find that the modeling of charge-parity oscillations is essential for a precise description of superconducting qubits. We emphasize that hardware dynamics often deviate from a Markovian model—qubit parameters drift and fluctuate on various timescales and are subject to interactions with uncontrolled degrees of freedom [59–61]. In fact, the accuracy of the model in the presented cases is encouraging and could even be considered as surprising. We therefore consider this model as a first approximation that should constitute the fundamental dynamical model and be further elaborated.

The presented simulation method is scalable to tens of qubits in a Markovian environment, provided that the structure of entanglement in the simulated states is limited as imposed by typical tensor-network constraints. For example, GHZ states serve as a standard benchmark of quantum computers and can also be efficiently simulated with MPSs, which holds for their dissipative dynamics as well [62]. The Hamiltonian and dissipative dynamics in many qubit devices are similar to those we have considered or can be accounted for with some modifications [63–68]. The realized graph state can be considered as a (simple) representative of a logical state of an error correction code [69]. We show that the underlying many-body dynamics generate decays and revivals of the stabilizers, reflecting the different contributions of coherent versus incoherent error mechanisms and emphasizing the importance of properly modeling them.

Our entire experiment and simulation software is accessible as open source [40] and can be used as a starting point for a detailed study of qubit dynamics during quantum error correction protocols.

[*] liran.shirizly@ibm.com
[†] gregoire.misguich@ipht.fr
[‡] haggaila@gmail.com

[1] J. Gambetta, Quantum-centric supercomputing: Bringing the next wave of computing to life (2022).
[2] F. Arute, K. Arya, R. Babbush, D. Bacon, J. C. Bardin, R. Barends, R. Biswas, S. Boixo, F. G. Brandao, D. A. Buell *et al.*, Nature (London) **574**, 505 (2019).
[3] S. Moses, C. Baldwin, M. Allman, R. Ancona, L. Ascarrunz, C. Barnes, J. Bartolotta, B. Bjork, P. Blanchard, M. Bohn *et al.*, arXiv:2305.03828.
[4] J. Wurtz, A. Bylinskii, B. Braverman, J. Amato-Grill, S. H. Cantu, F. Huber, A. Lukin, F. Liu, P. Weinberg, J. Long, S.-T. Wang, N. Gemelke, and A. Keesling, Aquila: Quera's 256-qubit neutral-atom quantum computer, arXiv:2306.11727.
[5] B. M. Terhal, Rev. Mod. Phys. **87**, 307 (2015).
[6] N. Sundaresan, T. J. Yoder, Y. Kim, M. Li, E. H. Chen, G. Harper, T. Thorbeck, A. W. Cross, A. D. Córcoles, and M. Takita, Nat. Commun. **14**, 2852 (2023).
[7] C. Ryan-Anderson, J. G. Bohnet, K. Lee, D. Gresh, A. Hankin, J. P. Gaebler, D. Francois, A. Chernoguzov, D. Lucchetti, N. C. Brown, T. M. Gatterman, S. K. Halit, K. Gilmore, J. A. Gerber, B. Neyenhuis, D. Hayes, and R. P. Stutz, Phys. Rev. X **11**, 041058 (2021).
[8] S. Krinner, N. Lacroix, A. Remm, A. Di Paolo, E. Genois, C. Leroux, C. Hellings, S. Lazar, F. Swiadek, J. Herrmann *et al.*, Nature (London) **605**, 669 (2022).
[9] L. Postler and S. Heußen, I. Pogorelov, M. Rispler, T. Feldker, M. Meth, C. D. Marciniak, R. Stricker, M. Ringbauer, R. Blatt *et al.*, Nature (London) **605**, 675 (2022).
[10] R. Acharya *et al.* Nature (London) **614**, 676 (2023).
[11] R. S. Gupta, N. Sundaresan, T. Alexander, C. J. Wood, S. T. Merkel, M. B. Healy, M. Hillenbrand, T. Jochym-O'Connor, J. R. Wootton, T. J. Yoder *et al.*, arXiv:2305.13581.
[12] J. Bylander, S. Gustavsson, F. Yan, F. Yoshihara, K. Harrabi, G. Fitch, D. G. Cory, Y. Nakamura, J.-S. Tsai, and W. D. Oliver, Nat. Phys. **7**, 565 (2011).

[13] H. Zhang, B. Pokharel, E. M. Levenson-Falk, and D. Lidar, Phys. Rev. Appl. **17,** 054018 (2022).

[14] P. Groszkowski, A. Seif, J. Koch, and A. A. Clerk, Quantum **7,** 972 (2023).

[15] E. Nielsen, J. K. Gamble, K. Rudinger, T. Scholten, K. Young, and R. Blume-Kohout, Quantum **5,** 557 (2021).

[16] K. X. Wei, I. Lauer, S. Srinivasan, N. Sundaresan, D. T. McClure, D. Toyli, D. C. McKay, J. M. Gambetta, and S. Sheldon, Phys. Rev. A **101,** 032343 (2020).

[17] Y. Y. Lifshitz, E. Bairey, E. Arbel, G. Aleksandrowicz, H. Landa, and I. Arad, arXiv:2112.10418.

[18] D. Puzzuoli, S. F. Lin, M. Malekakhlagh, E. Pritchett, B. Rosand, and C. J. Wood, J. Comput. Phys. **489,** 112262 (2023).

[19] T. Proctor, S. Seritan, K. Rudinger, E. Nielsen, R. Blume-Kohout, and K. Young, Phys. Rev. Lett. **129,** 150502 (2022).

[20] A. M. Green, T. Pandit, C. H. Alderete, N. M. Linke, and R. Uzdin, arXiv:2212.10771.

[21] J. P. Santos, I. Henao, and R. Uzdin, arXiv:2305.19359.

[22] A. Agarwal, L. P. Lindoy, D. Lall, F. Jamet, and I. Rungger, arXiv:2306.13021.

[23] K. X. Wei, E. Pritchett, D. M. Zajac, D. C. McKay, and S. Merkel, arXiv:2302.10881.

[24] M. Hein, J. Eisert, and H. J. Briegel, Phys. Rev. A **69,** 062311 (2004).

[25] M. Hein, W. Dür, J. Eisert, R. Raussendorf, M. Van den Nest, and H.-J. Briegel, in *Quantum Computers, Algorithms and Chaos* (IOS Press, Amsterdam, 2006), pp. 115–218.

[26] N. Kanazawa, D. J. Egger, Y. Ben-Haim, H. Zhang, W. E. Shanks, G. Aleksandrowicz, and C. J. Wood, J. Open Source Softwaare **8,** 5329 (2023).

[27] IBM Quantum, https://quantum-computing.ibm.com/ (2023).

[28] https://github.com/qiskit-community/lindbladmpo (2023).

[29] H. Landa and G. Misguich, SciPost Phys. Core **6,** 037 (2023).

[30] M. Fishman, S. White, and E. Stoudenmire, SciPost Physics Codebases 004 (2022).

[31] C. D. Wilen, S. Abdullah, N. Kurinsky, C. Stanford, L. Cardani, G. d'Imperio, C. Tomei, L. Faoro, L. Ioffe, C. Liu *et al.*, Nature (London) **594,** 369 (2021).

[32] K. Serniak, M. Hays, G. de Lange, S. Diamond, S. Shankar, L. D. Burkhart, L. Frunzio, M. Houzet, and M. H. Devoret, Phys. Rev. Lett. **121,** 157701 (2018).

[33] G. Catelani, R. J. Schoelkopf, M. H. Devoret, and L. I. Glazman, Phys. Rev. B **84,** 064517 (2011).

[34] D. Ristè, C. Bultink, M. J. Tiggelman, R. N. Schouten, K. W. Lehnert, and L. DiCarlo, Nat. Commun. **4,** 1913 (2013).

[35] D. M. Tennant, L. A. Martinez, K. M. Beck, S. R. O'Kelley, C. D. Wilen, R. McDermott, J. L. DuBois, and Y. J. Rosen, PRX Quantum **3,** 030307 (2022).

[36] B. G. Christensen, C. D. Wilen, A. Opremcak, J. Nelson, F. Schlenker, C. H. Zimonick, L. Faoro, L. B. Ioffe, Y. J. Rosen, J. L. DuBois, B. L. T. Plourde, and R. McDermott, Phys. Rev. B **100,** 140503(R) (2019).

[37] M. J. Peterer, S. J. Bader, X. Jin, F. Yan, A. Kamal, T. J. Gudmundsen, P. J. Leek, T. P. Orlando, W. D. Oliver, and S. Gustavsson, Phys. Rev. Lett. **114,** 010501 (2015).

[38] L. I. Glazman and G. Catelani, SciPost Phys. Lect. Notes 31 (2021).

[39] The experiments were run on the device ibm_cusco between 07/20/2023 and 07/27/2023. Data from the experiments are in [40]. Backends are listed in https://quantum-computing.ibm.com/.

[40] H. Landa, L. Shirizly, and Y. Ben-Haim, haggaila/graph-state-dynamics: Published version (v1.0.0) (2023) https://github.com/haggaila/graph-state-dynamics.

[41] See Supplemental Material at http://link.aps.org/supplemental/10.1103/PhysRevLett.132.010601 for more details about the model, results of the individual stabilizers, parameters values and the dynamical decoupling sequence.

[42] P. Krantz, M. Kjaergaard, F. Yan, T. P. Orlando, S. Gustavsson, and W. D. Oliver, Appl. Phys. Rev. **6,** 021318 (2019).

[43] J. Koch, T. M. Yu, J. Gambetta, A. A. Houck, D. I. Schuster, J. Majer, A. Blais, M. H. Devoret, S. M. Girvin, and R. J. Schoelkopf, Phys. Rev. A **76,** 042319 (2007).

[44] J. A. Schreier, A. A. Houck, J. Koch, D. I. Schuster, B. R. Johnson, J. M. Chow, J. M. Gambetta, J. Majer, L. Frunzio, M. H. Devoret, S. M. Girvin, and R. J. Schoelkopf, Phys. Rev. B **77,** 180502(R) (2008).

[45] K. X. Wei, E. Magesan, I. Lauer, S. Srinivasan, D. F. Bogorin, S. Carnevale, G. A. Keefe, Y. Kim, D. Klaus, W. Landers, N. Sundaresan, C. Wang, E. J. Zhang, M. Steffen, O. E. Dial, D. C. McKay, and A. Kandala, Phys. Rev. Lett. **129,** 060501 (2022).

[46] E. Magesan and J. M. Gambetta, Phys. Rev. A **101,** 052308 (2020).

[47] P. Jurcevic and L. C. G. Govia, Quantum Sci. Technol. **7,** 045033 (2022).

[48] A. McDonald and A. A. Clerk, Phys. Rev. Lett. **128,** 033602 (2022).

[49] H. Landa, D. Meirom, N. Kanazawa, M. Fitzpatrick, and C. J. Wood, Phys. Rev. Res. **4,** 013199 (2022).

[50] P. D. Nation, H. Kang, N. Sundaresan, and J. M. Gambetta, PRX Quantum **2,** 040326 (2021).

[51] D. M. Greenberger, M. A. Horne, and A. Zeilinger, in *Bell's Theorem, Quantum Theory and Conceptions of the Universe*, Fundamental Theories of Physics, edited by M. Kafatos (Springer Netherlands, Dordrecht, 1989), pp. 69–72.

[52] D. Gottesman, arXiv:quant-ph/9705052.

[53] J. R. Wootton, arXiv:2109.13308.

[54] C. Chamberland, G. Zhu, T. J. Yoder, J. B. Hertzberg, and A. W. Cross, Phys. Rev. X **10,** 011022 (2020).

[55] E. J. Zhang *et al.*, Sci. Adv. **8,** eabi6690 (2022).

[56] J. B. Hertzberg, E. J. Zhang, S. Rosenblatt, E. Magesan, J. A. Smolin, J.-B. Yau, V. P. Adiga, M. Sandberg, M. Brink, J. M. Chow *et al.*, npj Quantum Inf. **7,** 129 (2021).

[57] N. Dangniam, Y.-G. Han, and H. Zhu, Phys. Rev. Res. **2,** 043323 (2020).

[58] Z. Zhou, R. Sitler, Y. Oda, K. Schultz, and G. Quiroz, Phys. Rev. Lett. **131,** 210802 (2023).

[59] M. Carroll, S. Rosenblatt, P. Jurcevic, I. Lauer, and A. Kandala, npj Quantum Inf. **8,** 132 (2022).

[60] Y. Hirasaki, S. Daimon, T. Itoko, N. Kanazawa, and E. Saitoh, arXiv:2307.04337.

[61] T. Thorbeck, A. Eddins, I. Lauer, D. T. McClure, and M. Carroll, PRX Quantum **4**, 020356 (2023).

[62] J. Houdayer, H. Landa, and G. Misguich, arXiv:2305.17231.

[63] S. Cao, B. Wu, F. Chen, M. Gong, Y. Wu, Y. Ye, C. Zha, H. Qian, C. Ying, S. Guo *et al.*, Nature (London) **619**, 738 (2023).

[64] E. Bäumer, V. Tripathi, D. S. Wang, P. Rall, E. H. Chen, S. Majumder, A. Seif, and Z. K. Minev, arXiv:2308.13065.

[65] T. Graham, Y. Song, J. Scott, C. Poole, L. Phuttitarn, K. Jooya, P. Eichler, X. Jiang, A. Marra, B. Grinkemeyer *et al.*, Nature (London) **604**, 457 (2022).

[66] H.-X. Yang, J.-Y. Ma, Y.-K. Wu, Y. Wang, M.-M. Cao, W.-X. Guo, Y.-Y. Huang, L. Feng, Z.-C. Zhou, and L.-M. Duan, Nat. Phys. **18**, 1058 (2022).

[67] T. Monz, P. Schindler, J. T. Barreiro, M. Chwalla, D. Nigg, W. A. Coish, M. Harlander, W. Hänsel, M. Hennrich, and R. Blatt, Phys. Rev. Lett. **106**, 130506 (2011).

[68] C. Monroe, W. C. Campbell, L.-M. Duan, Z.-X. Gong, A. V. Gorshkov, P. W. Hess, R. Islam, K. Kim, N. M. Linke, G. Pagano *et al.*, Rev. Mod. Phys. **93**, 025001 (2021).

[69] A. Cross, G. Smith, J. A. Smolin, and B. Zeng, in *2008 IEEE International Symposium on Information Theory* (IEEE, New York, 2008), pp. 364–368.